Nonlinear Correction of the Direct Inverse Problem Solution in Real-Time Imaging

# Nonlinear Correction of the Direct Inverse Problem Solution in Real-Time Imaging

C. Origlia*†, D.O. Rodriguez-Duarte*, J.A. Tobon Vasquez*, N.K. Nikolova†, F. Vipiana*
*Dept. Electronics and Telecommunications, Politecnico di Torino, Torino, Italy,
{cristina.origlia, david.rodriguez, jorge.tobon, francesca.vipiana}@polito.it
†Dept. Electrical and Computer Engineering, McMaster University, Hamilton, ON, Canada, talia@mcmaster.ca

***Abstract*—This paper proposes a direct method for quantitative real-time imaging based on a nonlinear correction of the approximate linearized imaging kernel. The correction process relies on a pseudo-Rytov approximation employing the ratio between the total and incident fields in the scattering model, which can be estimated analytically. Unlike traditional iterative algorithms, there is no need for multiple computations of the direct scattering model, gaining computational speed and robustness to numerical inaccuracies. The procedure consists of two steps. First, a fast direct inversion algorithm based on the Born approximation provides the initial guess for the permittivity distribution; this study employs the Truncated Singular Value Decomposition (TSVD) and an in-house finite element-based solver to compute the imaging operator. Second, the field correction factor is transferred onto the object's permittivity to enhance its quantitative accuracy. The proposal viability is verified in 2D synthetic experiments at microwave frequencies, verifying improvements in the reconstructed unknown permittivity.**

***Index Terms*—Born approximation, electromagnetic scattering, microwave imaging, quantitative imaging, Rytov approximation.**

## I. Introduction

Microwave and millimeter-wave imaging explore various solutions for inspecting the electrical properties of optically opaque objects. The applications range from security screening [1] and packaged food control [2] to medical imaging, as in the case of breast tumor early detection [3] and brain stroke diagnosis [4]. These technologies often target real-time performance and quantitative outcomes, requiring optimized imaging strategies to balance computational speed and informative potential.

The direct inversion algorithms operate through linearized models of scattering, such as the one in the Born or Rytov approximations, resulting in fast reconstruction time [5]. The most common examples are radar-based methodologies, which capture only qualitative information about the dielectric contrast distribution, i.e., its shape and location [5]–[7]. Aiming to map the actual permittivity value, scattered-power mapping (SPM) and quantitative microwave holography (QMH) propose to add physical information measuring the system point spread function (PSF), i.e., the response to an electrically small scatterer of known volume and permittivity [8]–[10].

In contrast, the quantitative nonlinear methods employ high computational power in an iterative update of the permittivity estimate along with an update of the forward scattering model, where the field solution is obtained via electromagnetic (EM) simulations. In this process, difficulties may arise from convergence to unwanted local minima, which may depend on *a priori* information about the scatterer. Ensuring the accuracy of such information is challenging, especially in the biomedical context, where tissue complexity and variability between individuals preclude ideal modeling of the EM scenario. Traditional examples are the contrast source inversion (CSI) [11], [12], the distorted Born iterative methods (DBIM) [13], and the multistage procedures in [14]–[16]. To tackle the numerical burden, some authors have exploited high-speed parallel computing [17], but this is not always feasible. Recently, researchers have attempted faster solutions applying an optimized 2D finite element solver along with a suitably designed microwave tomography system [18]. In [19], the logarithmic transformation of the microwave algorithm leads to robust priors-independent convergence.

This work treats the nonlinearity of the EM problem in a direct inversion procedure based on Born's approximation (BA). In particular, it defines a correction factor that acts directly on the final output image to recover quantitative accuracy. The contribution stems from the statement of the ratio between the approximated and the actual total internal field, inspired by the exponential relationship in Rytov's approximation (RA) [5]. It comes down to a single-stage solution relative to the initial linear guess, avoiding the computational burden of iterative updates of the total field. Moreover, an analytical solution is available when the background Green function is known.

## II. Formulation

The procedure has two phases. First, a linear scattering model for fast inversion is applied, obtaining the initial guess, $\Delta\epsilon_0$, for the permittivity distribution. Then, the correction factor is derived and applied to obtain the enhanced image, compensating for the errors stemming from the BA of the total internal field.

The initial linearization relies on the zero-order BA, assuming that the dielectric contrast source is small enough to leave almost unperturbed the background field. However, in many practical cases, BA only partially reflects the actual imaging scenario, leading to significant quantitative errors and image artifacts, especially within the regions where the differences between total and incident field distributions are large [5].

The ill-posed linear problem needs to be inverted in a regularized fashion. Here, the truncated singular value decomposition (TSVD) scheme [20] is adopted. It obtains the unknown dielectric contrast function through the explicit formula:

$$\Delta\varepsilon_0 = \sum_{n=1}^{L_t} \frac{1}{\sigma_n} \langle \Delta S, u_n \rangle \, v_n, \tag{1}$$

where $\sigma_n$, $[u_n]$, and $[v_n]$ are the singular values, right and left singular vectors derived from the SVD of the discretized linear operator, respectively, and $L_t$ is the regularizing threshold.

As stated in [5], the scattering model in the frequency domain is written in terms of the measured scattered response $S^{\text{sc}}$ as

$$S_\zeta^{\text{sc}} = \frac{j\,\omega\,\varepsilon_0}{2\,a_\zeta} \iiint_{V_S} \Delta\varepsilon(\mathbf{r}') \mathbf{E}_{Rx}^{inc}(\mathbf{r}', \omega) \cdot \mathbf{E}_{Tx}^{tot}(\mathbf{r}', \omega) d\mathbf{r}', \tag{2}$$

where $\zeta$ indicates the response type, which reflects the transmitting and receiving antenna indices (i.e., $Tx, Rx = 1, ..., N_p$); $j$ is the imaginary unit; $\varepsilon_0$ is thepermittivity of free space; $\omega = 2\pi f$ is the angular frequency; $a_\zeta = a_{Rx} a_{Tx}$ is the incoming root-power waves product. In the integral, $\Delta\varepsilon$ is the relative permittivity contrast, $\mathbf{E}_{Rx}^{inc}(\mathbf{r}', \omega) = \mathbf{E}^{inc}(\mathbf{r}', \mathbf{r}_{Rx}, \omega)$ is the incident field due to the Rx antenna, and $\mathbf{E}_{Tx}^{tot}(\mathbf{r}', \omega) = \mathbf{E}^{tot}(\mathbf{r}', \mathbf{r}_{Tx}, \omega)$ is the total field due to the $Tx$ antenna, evaluated in each point $\mathbf{r}'$ in the imaging domain $V_S$.

Let us express the total field as

$$\mathbf{E}_{Tx}^{tot}(\mathbf{r}', \omega) \approx \mathbf{E}_{Tx}^{inc}(\mathbf{r}', \omega) \psi_{Tx}(\mathbf{r}', \omega), \tag{3}$$

where $\psi_{Tx}(\mathbf{r}', \omega)$ is a correction factor that can be transferred to the contrast permittivity distribution as follows:

$$S_\zeta^{\text{sc}} = \frac{j\,\omega\,\varepsilon_0}{2\,a_\zeta} \iiint_{V_S} \Delta\varepsilon(\mathbf{r}') \psi_{Tx}(\mathbf{r}', \omega) \mathbf{E}_{Rx}^{inc}(\mathbf{r}', \omega) \cdot \mathbf{E}_{Tx}^{inc}(\mathbf{r}', \omega) d\mathbf{r}'. \tag{4}$$

Thus, given the initial direct solution, $\Delta\varepsilon^{(0)}$, as previously discussed, and provided that we know $\psi_{Tx}(\mathbf{r}', \omega)$, the contrast can be obtained as

$$\Delta\varepsilon(\mathbf{r}') = \Delta\varepsilon^{(0)}(\mathbf{r}') / \psi_{Tx}(\mathbf{r}', \omega). \tag{5}$$

Here, it is worth noticing that $\psi_{Tx}(\mathbf{r}', \omega)$ is an implicit function of $\Delta\varepsilon$ given its dependence on $\mathbf{E}_{Tx}^{tot}(\mathbf{r}', \omega)$. Therefore, (5) is, in principle, nonlinear in $\Delta\varepsilon$. Moreover, the correction factor depends on $\mathbf{r}_{Tx}$, whereas $\Delta\varepsilon$ does not. Therefore, we need a unique optimal solution $\psi_o(\mathbf{r}', \omega)$, which ensures the fulfillment of (5) for all $Tx$.

In order to verify if such a solution is available, we can investigate the exact $\psi$ in simulation, computing the ratio of the total and incident fields in (3). Section III discusses the results of this analysis. In reality, we do not know the total field within the domain, in which case an analytical approximation of the total-to-incident field ratio can be pursued.

Adhering to the proposed corrected linear model, it can be shown that

$$\psi_{Tx}(\mathbf{r}', \omega) = 1 + k_0^2(\omega) \iiint_{V_S} \Delta\varepsilon(\mathbf{r}'') \psi_{Tx}(\mathbf{r}'', \omega) \mathcal{R}_{Tx}(\mathbf{r}', \mathbf{r}'', \omega) G_b(\mathbf{r}', \mathbf{r}'', \omega) d\mathbf{r}'', \tag{6}$$

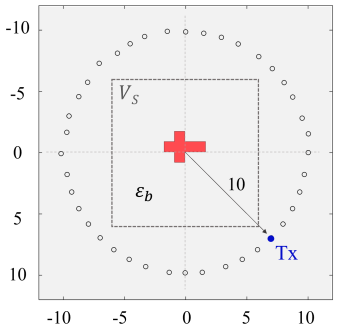


| Permittivity | Value |
|---|---|
| $\varepsilon_b = \varepsilon_b' - j\varepsilon_b''$ | 45.4−j13.9 |
| $\varepsilon_s = \varepsilon_s' - j\varepsilon_s''$ | 63.4−j28.3 |

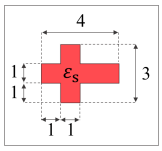


Fig. 1. Setup of the numerical experiment. The circles indicate the location of the probes surrounding the imaging domain, $V_s$. All dimensions are in cm.

where the function $\mathcal{R}_{Tx}$ indicates the scalar ratio between the incident fields at $\mathbf{r}'$ (observation point) and $\mathbf{r}''$ (source point). Considering a uniform background, the following approximation is employed:

$$\mathcal{R}_{Tx}(\mathbf{r}', \mathbf{r}'', \omega) \approx \frac{G_b(\mathbf{r}'' - \mathbf{r}_{\mathbf{Tx}}, \omega)}{G_b(\mathbf{r}' - \mathbf{r}_{\mathbf{Tx}}, \omega)}, \tag{7}$$

which relies on the assumption that the Tx antenna pattern cancels with no impact on the ratio. As a result, if $G_b$ is known, (6) leads to a simple direct solution for $\psi_{Tx}$. Then a strategy for its optimal estimate can be applied. A possible approach is indicated in the case study reported in Section III.

## III. Numerical Results

### A. Experiment design

The numerical experiment is designed through a 2D EM numerical model. The geometry is depicted in Fig. 1, consisting of a cross-shaped scatterer inside a uniform background, having complex relative permittivity $\varepsilon_s = 63.4 - j28.3$ and $\varepsilon_b = 45.4 - j13.9$, respectively, and a maximum size $l = 4$ cm. These example parameters are intended to represent brain hemorrhage imaging applications, as the one addressed by the authors in [21], which deals with the detection of small blood pooling ($\varepsilon_s$) inside the healthy brain tissue ($\varepsilon_b$).

The scene is sequentially illuminated through 40 point-like sources at 1.4 GHz. An in-house 2D solver based on the finite element method (FEM) computes the 40×40 scattering matrix [22]. It also provides the input to the TSVD imaging algorithm, and the electric field distributions inside the domain $V_s$, in the background alone (incident field) and in the presence of the scatterer (total field).

### B. Nonlinear correction results

From (3), it is possible to compute the distribution of $\psi_o$ in $V_s$, usually not available in experimental data. Here, the optimal solution has been selected as the averaged $\psi$ among all the $Tx$:

$$\psi_o(\mathbf{r}', \omega) = \frac{1}{N_p} \sum_{i=1}^{N_p} \psi_i(\mathbf{r}', \omega). \tag{8}$$

This strategy assumes that all contributions are equally weighted and summed for each point $\mathbf{r}'$, consistent with the imaging inversion scheme, but alternative ways may be investigated. Figure 2 shows the magnitude and phase of $\psi_0$. As expected, the ratio of the total and incident field values increases inside the dielectric contrast region and the nearby areas, where the scattered field is not negligible.

Then, the correction can be applied in the imaging process according to (5). As a reference, Fig. 3(a) shows the actual permittivity contrast of the imaged object, where the scatterer's contrast has real and imaginary parts equal to 18 and -14.4, respectively. Figure 3(b) shows the *ideal* TSVD reconstruction, which employs the actual integral kernel $\mathbf{E}^{inc}_{Rx} \cdot \mathbf{E}^{tot}_{Tx}$. The result is obtained with a threshold $L_t = -50$ dB, and it represents the best possible solution with this TSVD reconstruction algorithm. This result, too, can serve as a reference.

Finally, the initial guess $\Delta\varepsilon_0$ and its corrected counterpart $\Delta\varepsilon_{corr}$ are shown in Fig. 4. It is evident, that the corrected reconstructed permittivity is very similar to the ideal TSVD reconstruction, where the actual total internal field has been employed.

To quantify the improvement due to the proposed correction method, the root-mean-square error of the retrieved permittivity contrasts is calculated as

$$RMSE = \sqrt{\frac{1}{M}\sum_{m=1}^{M}[\Delta\epsilon_x(\mathbf{r}_m) - \Delta\epsilon_{tgt}(\mathbf{r}_m)]^2}, \qquad (9)$$

where $M$ is the number of pixels and the variable $\Delta\epsilon_x$ is the real or imaginary permittivity contrast of the studied cases (i.e., the initial guess, the correction, or the ideal case), compared to the target case ($\epsilon_{tgt}$). These results are listed in Table I. They confirm that a quantitative improvement is possible, with a major effect on the real part.

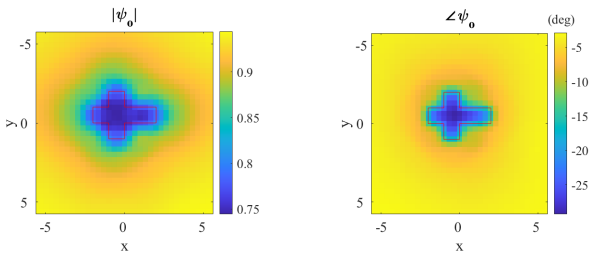


Fig. 2. (a) Magnitude and (b) phase of the correction factor, $\psi_o$.

TABLE I
RMSE WITH RESPECT TO THE TARGET PERMITTIVITY CONTRAST

| | Real part | Imaginary part |
|---|---|---|
| $\Delta\varepsilon_0$ | 2.40 | 0.94 |
| $\Delta\varepsilon_{corr}$ | 1.11 | 1.10 |
| $\Delta\varepsilon_{ideal}$ | 0.80 | 0.83 |

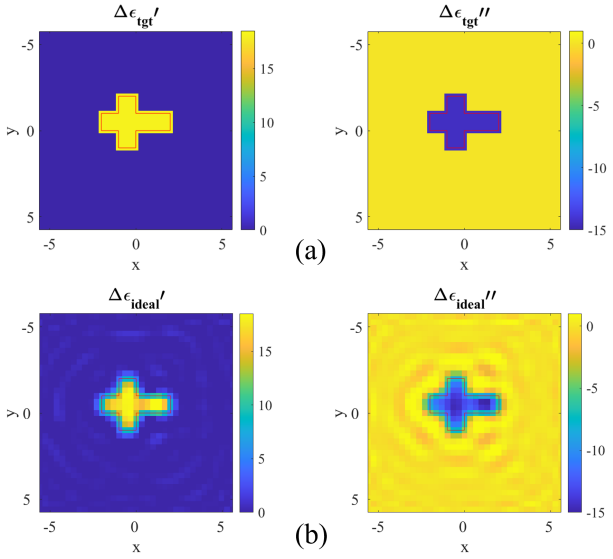


Fig. 3. (a) Real (left) and imaginary (right) parts of the target permittivity contrast and (b) the corresponding ideal reconstruction using TSVD inversion scheme. Axis dimensions are in cm.

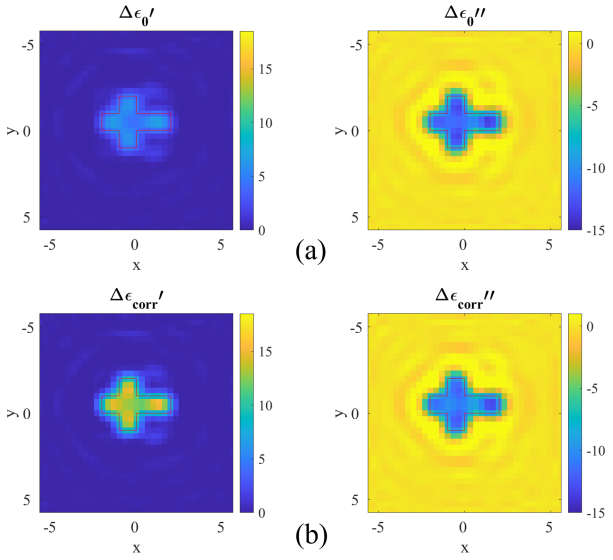


Fig. 4. (a) Real (left) and imaginary (right) parts of the initial guess of the TSVD algorithm employing the Born approximation and (b) the reconstruction obtained by applying $\psi_o$ correction. Axis dimensions are in cm.

## IV. Conclusion and Perspectives

This work addresses an innovative strategy in real-time EM inverse scattering, aiming to recover quantitative information lost through the direct inversion process using a correction variable that accounts for nonlinearities. Furthermore, it proposes an original approach to an optimal simulation-free direct solution via analytical derivation of the internal fields, since these fields are usually not available in real-life applications such as microwave imaging. The numerical validation demonstrates the possibility of recovering significant quantitative information, and the relative improvement is expected to increase when the Born accuracy limitation is strongly violated.

Future work is devoted to completing the development of an explicit analytical formulation of the designed procedure and testing it for efficient fast inversion. Moreover, it is planned to extend the analysis to the 3D configuration in view of the validation in real imaging applications.

## V. Acknowledgments

This research was supported in part by the project PON Research and Innovation "Microwave Imaging and Detection powered by Artificial Intelligence for Medical and Industrial Applications" (DM 1062/21), funded by the Italian Ministry of University and Research (MUR), and it was carried out partially within the Agritech National Research Center, funded by the European Union Next-Generation EU (Piano Nazionale di Ripresa e Resilienza (PNRR) – MISSIONE 4 COMPONENTE 2, IN- VESTIMENTO 1.4 – D.D. 1032 17/06/2022, CN00000022). Additionally, it was funded by the Natural Sciences and Engineering Research Council of Canada (NSERC), grant numbers RTI-2020-00456, RGPIN-2017-06058, and RGPIN-2023-04483.

## References

[1] Y. Meng, C. Lin, J. Zang, A. Qing, and N. K. Nikolova, "General theory of holographic inversion with linear frequency modulation radar and its application to whole-body security scanning," *IEEE Transactions on Microwave Theory and Techniques*, vol. 68, no. 11, pp. 4694–4705, 2020.

[2] J. A. Tobon Vasquez, R. Scapaticci, G. Turvani, M. Ricci, L. Farina, A. Litman, M. R. Casu, L. Crocco, and F. Vipiana, "Noninvasive inline food inspection via microwave imaging technology: An application example in the food industry," *IEEE Antennas and Propagation Magazine*, vol. 62, no. 5, pp. 18–32, 2020.

[3] L. Guo, A. S. M. Alqadami, and A. Abbosh, "Stroke diagnosis using microwave techniques: Review of systems and algorithms," *IEEE Journal of Electromagnetics, RF and Microwaves in Medicine and Biology*, vol. 7, no. 2, pp. 122–135, 2023.

[4] M. A. Aldhaeebi, K. Alzoubi, T. S. Almoneef, S. M. Bamatraf, H. Attia, and O. M. Ramahi, "Review of microwaves techniques for breast cancer detection," *Sensors*, vol. 20, no. 8, 2020.

[5] N. K. Nikolova, *Introduction to Microwave Imaging*. EuMA High Frequency Technologies Series, Cambridge University Press, 2017.

[6] A. Trakic, A. Brankovic, A. Zamani, N. Nguyen-Trong, B. Mohammed, A. Stancombe, L. Guo, K. Bialkowski, and A. Abbosh, "Expedited stroke imaging with electromagnetic polar sensitivity encoding," *IEEE Transactions on Antennas and Propagation*, vol. 68, no. 12, pp. 8072–8081, 2020.

[7] D. Byrne, M. O'Halloran, M. Glavin, and E. Jones, "Data independent radar beamforming algorithms for breast cancer detection," *Progress In Electromagnetics Research*, vol. 107, pp. 331–348, 2010.

[8] D. Tajik, R. Kazemivala, and N. K. Nikolova, "Real-time imaging with simultaneous use of born and rytov approximations in quantitative microwave holography," *IEEE Transactions on Microwave Theory and Techniques*, vol. 70, no. 3, pp. 1896–1909, 2022.

[9] D. S. Shumakov and N. K. Nikolova, "Fast quantitative microwave imaging with scattered-power maps," *IEEE Transactions on Microwave Theory and Techniques*, vol. 66, no. 1, pp. 439–449, 2018.

[10] R. Kazemivala, D. Tajik, and N. K. Nikolova, "Simultaneous use of the born and rytov approximations in real-time imaging with fourier-space scattered power mapping," *IEEE Transactions on Microwave Theory and Techniques*, vol. 70, no. 5, pp. 2904–2920, 2022.

[11] P. M. van den Berg and A. Abubakar, "Contrast source inversion method: State of art," *Progress in Electromagnetics Research-pier*, vol. 34, pp. 189–218, 2001.

[12] V. Mariano, J. A. Tobon Vasquez, and F. Vipiana, "A novel discretization procedure in the csi-fem algorithm for brain stroke microwave imaging," *Sensors*, vol. 23, no. 1, 2023.

[13] L. Guo, M. Khosravi-Farsani, A. Stancombe, K. Bialkowski, and A. Abbosh, "Adaptive clustering distorted born iterative method for microwave brain tomography with stroke detection and classification," *IEEE Transactions on Biomedical Engineering*, vol. 69, no. 4, pp. 1512–1523, 2022.

[14] T. Rubaek, P. M. Meaney, P. Meincke, and K. D. Paulsen, "Nonlinear microwave imaging for breast-cancer screening using gauss–newton's method and the cgls inversion algorithm," *IEEE Transactions on Antennas and Propagation*, vol. 55, no. 8, pp. 2320–2331, 2007.

[15] C. Estatico, A. Fedeli, M. Pastorino, and A. Randazzo, "Quantitative microwave imaging method in lebesgue spaces with nonconstant exponents," *IEEE Transactions on Antennas and Propagation*, vol. 66, no. 12, pp. 7282–7294, 2018.

[16] N. Abdollahi, I. Jeffrey, and J. LoVetri, "Improved tumor detection via quantitative microwave breast imaging using eigenfunction-based prior," *IEEE Transactions on Computational Imaging*, vol. 6, pp. 1194–1202, 2020.

[17] P.-H. Tournier, M. Bonazzoli, V. Dolean, F. Rapetti, F. Hecht, F. Nataf, I. Aliferis, I. El Kanfoud, C. Migliaccio, M. de Buhan, M. Darbas, S. Semenov, and C. Pichot, "Numerical modeling and high-speed parallel computing: New perspectives on tomographic microwave imaging for brain stroke detection and monitoring," *IEEE Antennas and Propagation Magazine*, vol. 59, no. 5, pp. 98–110, 2017.

[18] S. Hosseinzadegan, A. Fhager, M. Persson, S. D. Geimer, and P. M. Meaney, "Discrete dipole approximation-based microwave tomography for fast breast cancer imaging," *IEEE Transactions on Microwave Theory and Techniques*, vol. 69, no. 5, pp. 2741–2752, 2021.

[19] S. D. G. Paul M. Meaney and K. D. Paulsen, "Two-step inversion with a logarithmic transformation for microwave breast imaging," *Med. Phys.*, vol. 44, pp. 4239–4251, 2017.

[20] M. Bertero and P. Boccacci, *Introduction to Inverse Problems in Imaging*. CRC Press, Taylor & Francis Group, 1998.

[21] D. O. Rodriguez-Duarte, C. Origlia, J. A. T. Vasquez, R. Scapaticci, L. Crocco, and F. Vipiana, "Experimental assessment of real-time brain stroke monitoring via a microwave imaging scanner," *IEEE Open Journal of Antennas and Propagation*, vol. 3, pp. 824–835, 2022.

[22] D. O. Rodriguez-Duarte, J. A. T. Vasquez, R. Scapaticci, L. Crocco, and F. Vipiana, "Assessing a microwave imaging system for brain stroke monitoring via high fidelity numerical modelling," *IEEE Journal of Electromagnetics, RF and Microwaves in Medicine and Biology*, vol. 5, no. 3, pp. 238–245, 2021.